A Holistic Approach for Spatial Mapping of Hair Surface Properties of Ethnic Indian Hair

Mandal, Ranju Prasad*; Hensel, Marie; Hansen, Leonie; Kessler-Becker, Daniela

Henkel Beauty Care Disruptive Technologies, Henkel AG & Co. KGaA, Düsseldorf, Germany
Henkelstrasse 67, 40589, Düsseldorf, Germany, Phone: +49-211-7972699;
*E-Mail: ranju.mandal@henkel.com

Abstract

Background: This is probably the first study on a detail investigation of chemically untreated Indian hair using different analytical techniques that establishes a correlation between the methods to understand the hair structure during fiber aging.

Methods: Untreated Indian Hair, shaved at the scalp, was divided into separate parts along the length as root, length, and tip. These different parts were analyzed with modern analytical techniques like LSM, SEM, ATR-FTIR, streaming zeta potential, XPS, TGA.

Results: LSM and SEM studies showed more cuticular damage and decrement in cellular deposits proceeding from root to tip. ATR-FTIR studies between root and tip hair showed distinct changes in $-CH_2$, $-SO_3$ stretching and a shift in amide spectra. Deconvoluted amide spectrum showed the change in relative amounts of different protein conformations on proceeding from root to tip. Substantial change in the streaming zeta potential and the isoelectric point (IEP) were observed in these regions. TGA studies also indicated the difference in spatial conformation.

Conclusions: This study provided new insights on the spatial distribution of properties like protein conformation, permeability, zeta potential, presence of different biological substances etc. along the hair length. By combining different methods and using untreated Indian hair as a model fiber, a set of tools was established that helps monitoring fiber ageing. This study helps to understand the hair surface more clearly and opens new possibilities to overcome obstacles related to hair color, style, and care formulations.

Keywords: ATR-FTIR; Indian hair; Streaming Zeta Potential; Protein Conformation; LSM

Introduction.

Hair has a proteinaceous, and filamentous structure [1, 2]. Its primary role is to protect the body against heat or cold. Although in humans the role of hair has evolved, and it has become an integral part of beauty concepts regardless of ethnicity. However, the role of hair is not only limited to beauty concepts. As history shows, hair has also become a language for expression, freedom, and strength [3].

Hair consists of mainly cuticle and cortex, and in some cases the medulla in the center [4]. The cortex represents most of the hair fiber composition and thus controls a majority of the physical and mechanical properties of hair [1]. Cortex is composed of dead cells, which are mainly filled with keratinous protein [5]. The keratin contains a high cystine content, an amino acid that has the capacity to cross-link the protein in the α-helix by intermolecular disulfide bonds [6]. The cuticle is the outermost region of the hair fiber, it protects the cortex. It consists of flat overlapping cells arranged like tiles in the root-to-tip direction. The cuticle in human hair consists of approximately 5–10 layers of scales. Each cuticle cell is generally 0.3–0.5 mm thick with the visible length being about 5–10 mm [7]. The diameters of human hair fibers range between 50–100 mm, depending on the ethnicity. They consist of various sub-layered structures like epicuticle, A-layer, exocuticle and endocuticle, inner layer and the cell membrane complex in between cells. The epicuticle layers are covered by a hydrophobic fatty acid layer, known as β-layer, comprising of 18-methyl eicosanoic acid (18-MEA) [7, 8]. This 18-MEA layer is chemically grafted to the amorphous keratin through a thioester linkage and acts as a protective barrier against water penetration [9].

 From an ethnic point of view, hair is divided into three main categories: Asian, African, and Caucasian [10]. Among them, Asian hair has different types of diversity, however, currently available literature is mainly focused on east Asian hair. On the other hand, southeast Asians hair i.e. the hair type of the Indian subcontinent, still suffers from limited scientific information [11]. But Indian hair is used for wigs and extensions worldwide due to their undamaged nature and thus deserves special attention and needs more research to explore it further. In India, the importance of hair is more prominent and deeply rooted in culture. With very important historical and mythological reference, hair became a strong metaphor related to every religion evolved in this subcontinent and their rituals. As a result, to women in rural India, hair is considered as such an auspicious element of their life that

they avoid any chemical treatments [12]. This, incidentally, leads us to a great source of chemically untreated hair for detailed study.
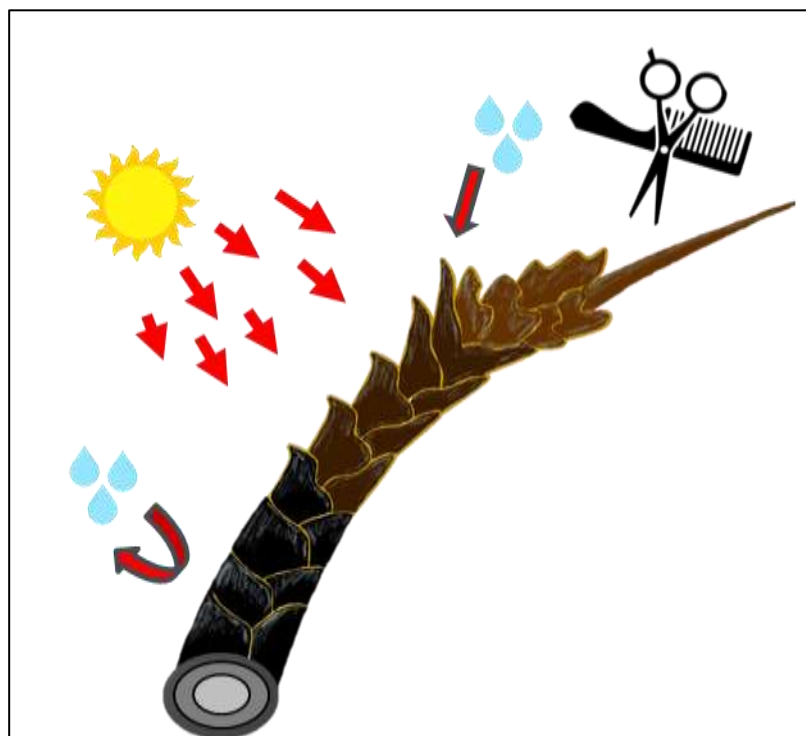

Fig. 1. Effect of different external stimuli on hair surface

Hair, after its generation from hair folicles, travels a long journey through growth regression and resting phases [13]. Throughout time, hair experiences many physical and chemical changes as it is exposed to a multitude of different factors of daily life. Studies report the effect of different stimuli, such as UV light, combing, and other mechanical treatments like drying, washing etc. (**Fig. 1**). These external forces create physical and chemical changes in hair [14-17]. None of these reports are focused on systematically studying hair aging, specifically the Indian hair type. In this work, we carry out a detailed analysis with different batches of Indian hair using some well-known and some less explored analytical techniques. During this process, the properties along the hair from root to tip were studied to get an overview on the morphological and the chemical changes throughout the aging process and, most importantly to find out the correlation between these characteristics. This study aims not only to understand the hair surface more vividly but to pave the way to future hair applications.

Materials and Methods.

Indian Hair samples were obtained from Kerling International Haarfabrik GmbH, Germany. The braids were shaved at the scalp have a length of 20 cm and weighed 46 g. A whole braid of hair from a single person was used. All hair samples were cleaned properly with 10% SLS solution adjusted at pH 10. For measurement of root, length, and tip they are cut into separate parts. Starting from the top, first and last 5 cm are marked as root and tip and the 10 cm at the middle marked as length. For microscopic measurements (LSM, SEM and AFM) single fibers were used and for other measurements single braids were used for analysis and all measurements done in triplicates.

Microscopic images of the hair were taken with the 3D measuring laser microscope LEXT OLS5000 by Olympus K.K. recorded with the associated data acquisition software. This enables recordings with 50x and 100x magnifications. AFM studies were done using Tosca 400 from Anton Paar. For the AFM measurements, each measurement was made in tapping mode. The samples were cut and placed on double sided tape with tweezers. SEM measurements were done in FeiNovaNanoSEM450 instrument in the SE (Secondary Electrons) mode. This mode correlates to the topography of the samples. They were again prepared with tweezers and placed in a mold to harden in an epoxy resin. The NIR measurement was carried out with the Brucker MPA II multipurpose analyzer. XPS studies were done in ESCALAB 250Xi from Thermo Scientifico Scientific. ATR-FTIR measurements were carried out with a Perkin Elmer Spectrum 100 device in UATR mode. The spectra were resolved into principal components using Specwin software. The SurPASS 3 from Anton Paar was used to measure the zeta potential. Ultrapure water from the Milli-Q® Advantage A10 water purification system from Merck was used for the measurements. For weighing XP5003S Delta Plus (d=1mg) from Mettler Toledo was used. TGA studies were done in TGA Q5000 IR from TA Instruments.

Results

Fig. 2(A-C) presents the laser microscopic images of Indian hair in root, length, and tip. In the root area of the Indian hair (**Fig. 2A**), it is observed that the hair surface is regular and smooth, cuticles are undamaged. The presence of some oily, lipid-like substance has been observed. In contrast, in the length part of the hair (**Fig. 2B**), no such oily deposits are

present, but, at the same time, due to more external exposure, the edges of cuticles are lifted to some extent and cuticular damage was also observed. Proceeding further to **Fig. 2C**, this represents the tip edge of the hair, it shows that the cuticles are almost completely removed. A damaged and bare cortex structure is observed indicating the high damage level at this part of the hair.
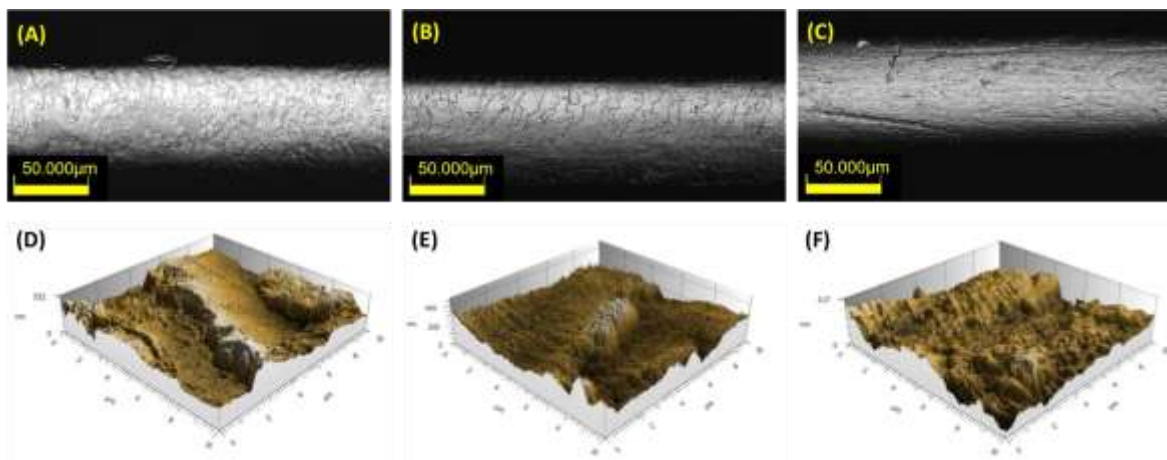

Fig. 2 LSM (A-C) and AFM images (D-F) of the Indian hair showing root, length and tip, respectively.

The AFM study gives an idea about the three-dimensional topographies of hair. **Fig. 2D** shows the root region, clearly indicating the step-like pattern of the cuticular structure, one overlying the another. Some deposition of lipids, especially at the intersection of two cuticles, is also observed. Overall, the cuticular structure can be described as quite regular whereas in **Fig. 2E** the step-like pattern in the cuticle layer is still observed, but those seems quite roughened with the broken scale edges indicating surface damage. In the AFM image of the tip (**Fig. 2F**) no such stepwise pattern of the cuticle cells can be observed.
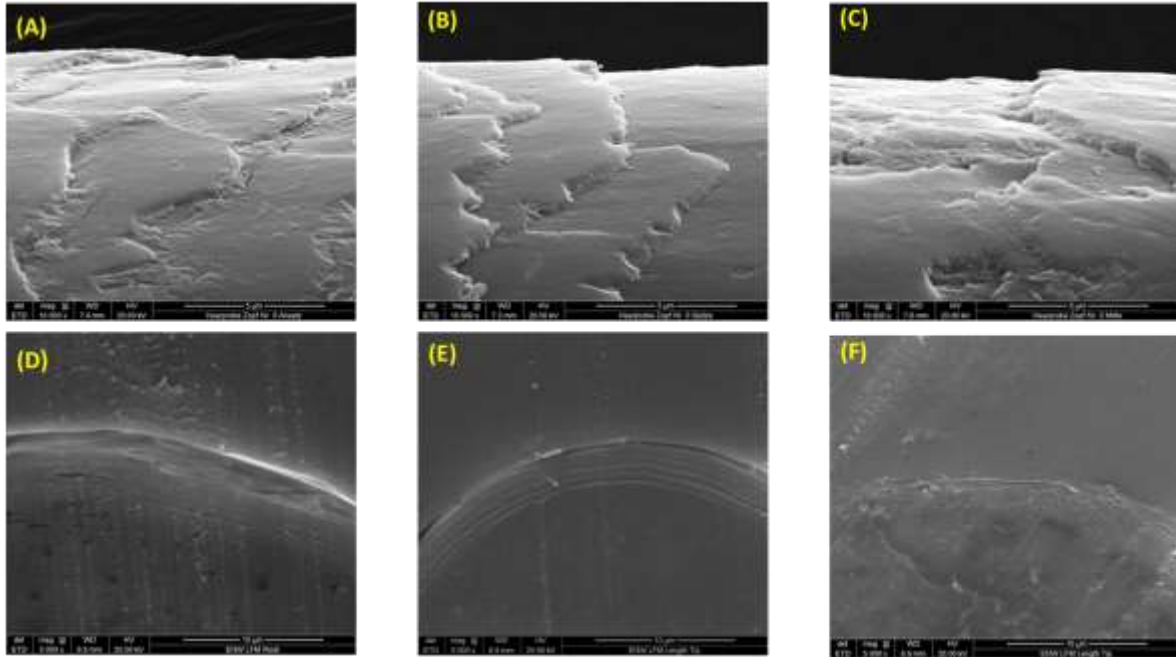
Fig. 3 SEM images of Indian hair showing surface morphology (A-C) and longitudinal cross section (D-E) of root, length and tip, respectively.

SEM studies were also carried out on different parts of the Indian hair to get a more detailed understanding of the surface morphology. **Fig 3A** represents the root hair. It shows intact cuticles overlying one another and some deposits observed mainly at the overlapping region. The length (**Fig. 3B**) shows a much cleaner surface. Like the LSM and AFM images, the SEM results also suggest a very damaged cuticular surface at the tip (**Fig. 3C**). **Fig. 3D-F** shows SEM images of hair cross sections. **Fig. 3D** clearly indicates the compact overlapping layers of cuticles beneath the thick layer of lipids on the surface. But in the length region, this thick protecting layer is completely absent, and cuticle cells are more clearly visible (**Fig. 3E**). Proceeding towards the tip, **Fig. 3F** shows most of the cuticle layers being removed and mostly the cortex structure.
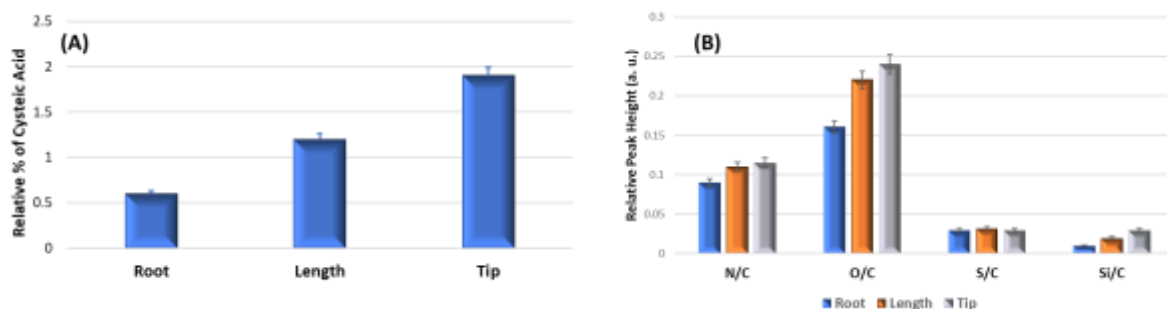
Fig. 4(A) Relative change of cysteic acid concentration obtained from NIR measurement and, (B) elemental distribution of N, O, S and Si as obtained from XPS analysis of root, length and tip of Indian hair, respectively.

Estimating cysteic acid in hair using NIR spectroscopy has been one of the most common methods to determine its damage level. **Fig. 4A** shows there is a systematic increase of cysteic acid amount from root to tip. XPS was also used to analyze the hair surface as it is very sensitive towards this structure and is commonly used to get detailed chemical compositional information. As observed in **Fig. 4B**, the elemental distribution on the hair surface is very heterogeneous with an appreciable increase of the oxygen and silicon from root to tip. **Table 1** gives an idea of the change in contribution of different functional groups on the hair surface. There is an appreciable decrease in the C-C/C-H units. At the same time, the amount of cystine decreases and that of cystine dioxide increases.

Table 1. Amount (%) of different elements in root, length and tip of Indian hair as obtained from XPS analysis.

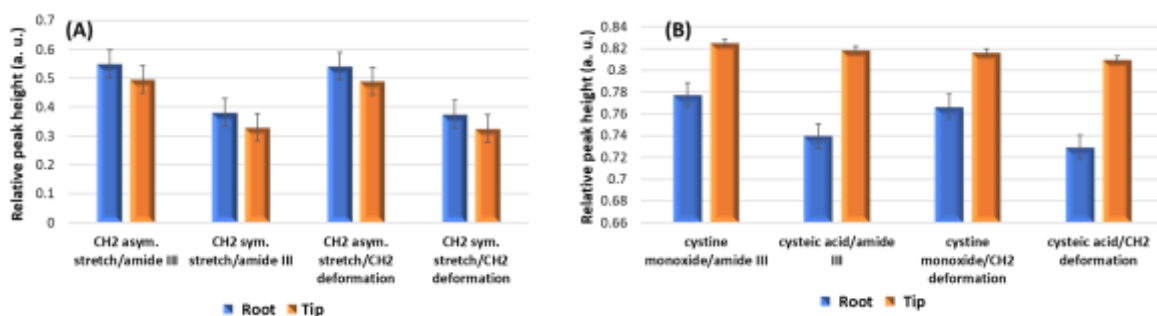| Element	Hair Root	Hair Length	Hair Tip
C-C / C-H (%)	81.7	72.7	72.6
C-OR / -NR (%)	7.3	16.0	14.6
C=O (%)	7.6	7.0	9.1
C-OOR (%)	3.5	4.3	3.7
Cystein/Cystin (%)	100.0	87.3	81.6
SO_2 (%)	-	12.7	18.4

Fig. 5(A) Relative change in intensity of CH₂ stretching signals and (B) cystine oxidation analogs as obtained from ATR-FTIR measurement of root and tip of Indian hair. Amide III band and CH₂ deformation are used as internal standards.

Another surface-based technique, ATR-FTIR with a penetration depth of ~10 µm and thus able to show the cuticle and part of the cortex, was also used. The results are shown in **Fig. 5**. Comparison of ATR-FTIR spectra of the root and tip of hair showed chemical changes mostly at wavenumbers 2918, 2850, 1182, and 1040 cm^{-1}. These bands correspond to CH$_2$ asymmetric stretching, CH$_2$ symmetric stretching, cystine monoxide and cysteic acid. These bands are seen as indicators for changes in the surface vicinity whereas the amide III band (1235 cm^{-1}) and CH$_2$ deformation (1451 cm^{-1}) are used as internal standards. **Fig. 5A** shows the change in CH$_2$ symmetric and asymmetric stretching, indicating a higher contribution of surface lipids in the root compared to the tip. A completely opposite trend for cysteic acid and cysteine monoxide can be found (**Fig. 5B**). Interestingly, a shift towards a higher wavenumber for amide I (1660 cm^{-1}) and amide II (1520 cm^{-1}) bands was observed as we moved from root to tip of the Indian hair. These shifts indicate the change in protein conformation during aging of the hair. To understand this protein conformational change better, the bands were deconvoluted (**Fig. 6A-B**) and the relative amounts of the different protein conformation viz. α-helix, β-sheet and random coil were determined. The result shows that the relative contribution of random coil increases whereas that of β-sheet decreases; the amount of α-helix conformation seems less affected (**Fig. 6C**).
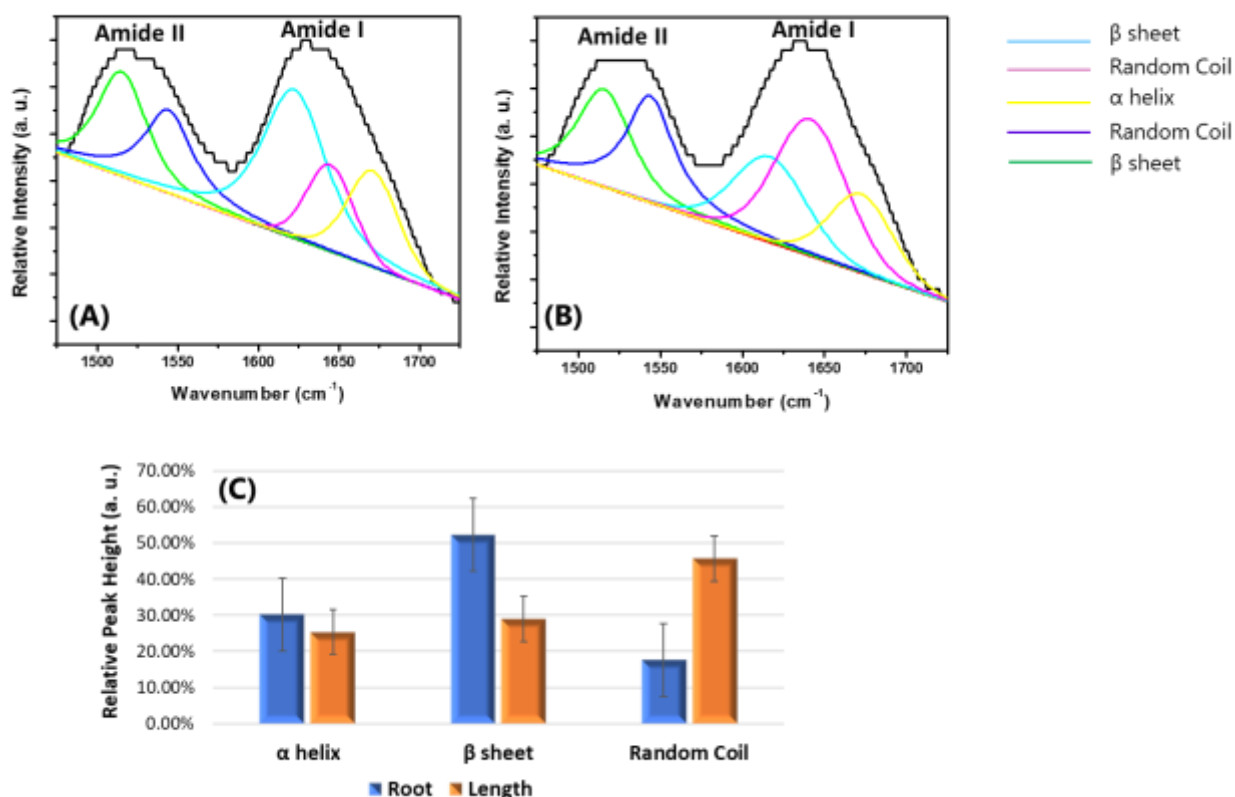
Fig. 6(A-B) Deconvoluted spectra of amide I and amide II bands of ATR-FTIR spectra and corresponding (C) relative change in different protein conformations of Indian hair in root and tip, respectively.

ATR-FTIR spectroscopy was also used to get an overview of the distribution of the melanin population on the upper cortex layer along the hair length by a non-destructive method. For this, spectra of different parts of Indian hair were subtracted by the spectra of grey hair that reportedly contains a negligible amount of melanin and the relative intensity of pheomelanin and eumelanin was determined (**Fig. 7A**). According to Stanic et al., the IR bands at ~1220 and ~1650 cm^{-1} can be characterized for pheomelanin and eumelanin, respectively [18]. Indian hair, due to its natural black color, contains predominantly eumelanin, hence the peak for eumelanin is more prominent than that of the pheomelanin band. Careful monitoring of the subtraction spectra shows a clear reduction in intensity for the eumelanin band from root to tip whereas the band for pheomelanin seems less affected.
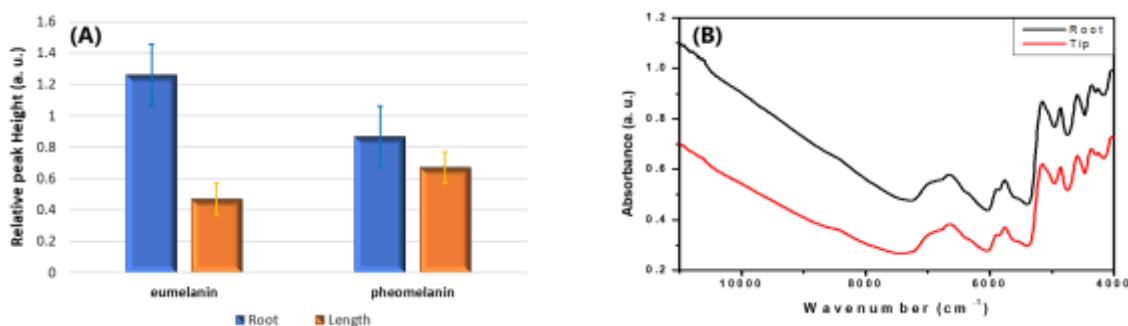
Fig. 7(A) Relative intensity of eumelanin and pheomelanin peaks as obtained from the subtracted ATR-FTR spectra of Indian hair and grey hair, (B) NIR spectrogram of Indian hair.

To get further substantiation, NIR spectra for the root and the length of the hair were also recorded (**Fig. 7B**). The area between 7500-10000 cm^{-1} is reported to show the signal for eumelanin [19] that was found to be decreasing, moving from root to tip.
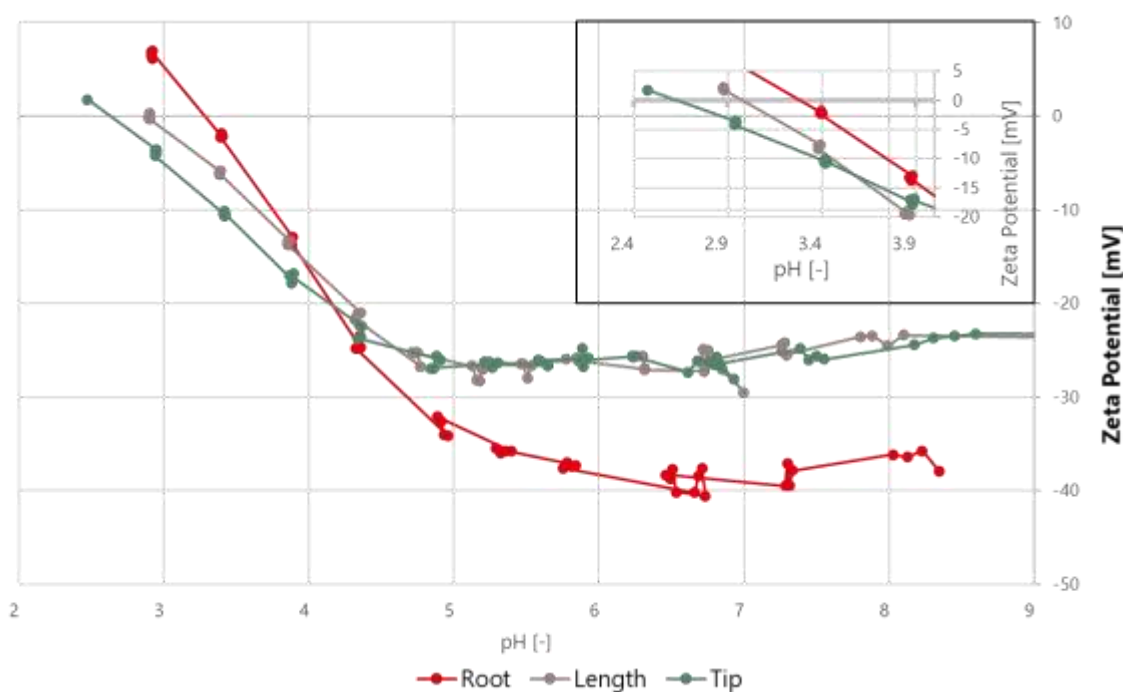

Fig. 8 Streaming zeta potential curves for different parts of Indian hair. Inset showing the corresponding IEPs.

Fig. 8 shows the streaming zeta potential over the pH for different parts of the Indian hair. This analytical method is much less explored for hair characterization. The curves of the different parts of hair over the pH range of approximately 2.5 to 8 can be seen in the figure. There is a clear distinction between the curves for root to length and tip. The streaming zeta potential value at pH 8 is different depending on the part of hair. For the root, it starts at -42 mV and remains almost constant up to a pH of 5.5. Then, the curve rises steeply and ends in the IEP. The curves for length and tip on the other hand start at -24 mV and remain constant up to pH 4.5. Then the slopes increase sharply until they reach their respective IEPs. The inset shows the IEPs for these different parts. There is a systematic decrease in IEP from 3.3 for the root to 2.7 for the tip.
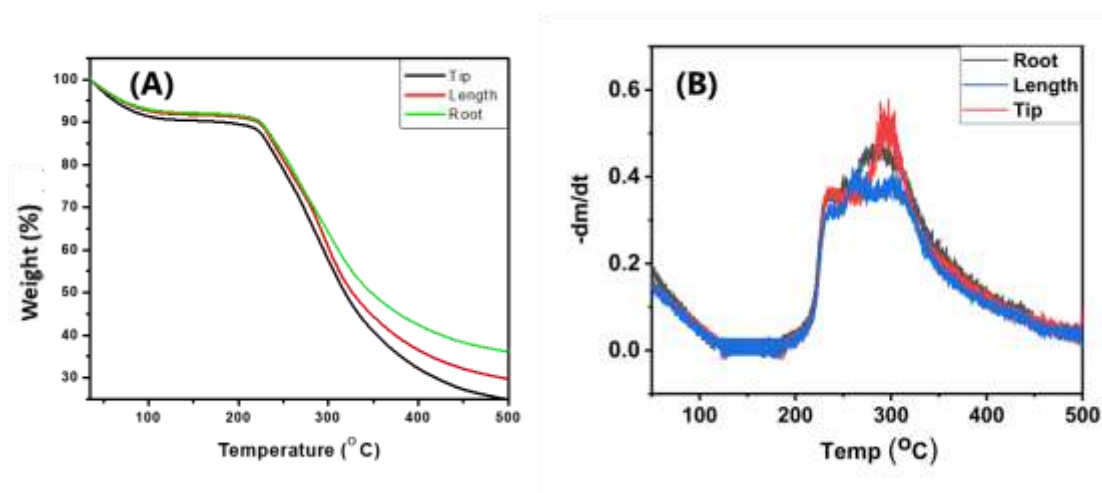

Fig. 9 (A)TG curves and (B) corresponding first derivative spectra for root, length, and tip of Indian hair.

Fig. 9(A) shows the TG curves for the root, length, and tip of the Indian hair. TG studies were carried out to understand the thermal stability of the hair parts that, in turn, depends on the internal structure of the hair. At a controlled heating rate, stepwise mass change was observed for all hair samples with the increasing temperature. It is clearly observed that although the trend of their thermal decomposition is similar, there is a difference in the decomposition rate. The decomposition rate increases from root to tip in a systematic way. **Fig. 9(B)** show the first derivative spectra of the TG curves. In general, for hair samples, the first mass loss stage observed can be attributed to the water release in the range of 25–131°C. The second and third mass loss stages are related to the denaturation of

hair keratin, with organic degradation of hair microfibrils and matrix, at around 280, 320 and 350°C. In the temperature range of 350–550°C the complete degradation of the hair keratin carbonic chains takes place. It was observed that the root hair presents more loss stages for hair degradation compared to the tip hair. This is more clearly evidenced in the first derivative of the TG spectra.

Discussion.

From the morphological characterizations like LSM, AFM and SEM for the root hair, it could be observed that hair has a multilayered structure. Those cuticular layers are again protected by surface lipids and fatty acids, the major constituent of which is 18-MEA. This hydrophobic layer protects the hair from external aging stress [7, 9]. As an effect of multiple daily stresses, including chemical and mechanical treatments, the lipid composition of hair was notably changed [14-17]. As observed in the LSM studies (**Fig. 2A-C**), the loss in lipid concentration not only made the hair surface cleaner but also exposed it to extensive weathering. This leads to observable cuticle damage and finally resulted in lifted cuticle edges and a significant amount of exposure of the endocuticle at the length of the hair. With the progression of hair aging, the multitude of physical stresses increased to large extents. This ultimately caused the cuticles to flake and strip away and lead to almost a bare cortex at the tip. These phenomena are completely substantiated by AFM and SEM images (**Fig. 2D-F, 3**).

The removal of surface lipids also modulates the chemical nature of the hair surface. The hydrophobic long chain 18-MEA is attached by covalent thioester bonds at the outer edge of the cuticle with the underlying protein layer. With the stripping of the outer lipid layer, the thioester bond will undergo subsequent oxidation as observed from the increase in the percentage of cysteic acid in NIR and FTIR measurement (**Fig. 4A**) with hair aging [20]. ATR-FTIR spectra not only support the results observed from morphological characterization of hair but also help to get a clearer picture. The change in the -CH$_2$ stretching frequencies can be correlated well with the reduction in the surface lipid amount from root to tip (**Fig. 5**) [21]. This is again concerted with the increase in the amount of cysteic acid [21, 22].

From XPS one can get a clearer idea on elemental mapping on hair surface (**Fig. 4B**) [22-24]. XPS studies support the theory of lipid removal from root to tip as the relative amount of C-C/C-H, corresponding to the surface lipids, decreases from root to tip (**Table 1**) and the relative amount of oxygen increases indicating surface oxidation [24] and oxidative cleavage of the disulphide bonds as also observed from NIR measurement. The increase in relative concentration of silicon can be correlated with the fact that the tip region is more hydrophilic. That promotes better absorption of the silicon-containing care ingredients which are generally present in hair care formulations.

This surface lipid stripping by weathering also affects the underlying protein structure. As can be observed in **Fig. 6**, the relative contribution of ordered protein conformations like α-helix and β-sheet decreases and that of the more irregular random coil conformation increases. These results indicate that the tip part of the Indian hair has a more chemically disordered conformation than the root. A recent study also reports on the change in protein conformation along the surface of cuticle cells [8]. As can be seen in **Fig. 7**, weathering also has an immense effect on melanin pigment degradation. Both FTIR and NIR measurements indicate that eumelanin concentration decreases markedly from root to tip. Previous literature shows that eumelanin has relatively less chemical stability than pheomelanin and degrades faster on exposure to sunlight [25]. This phenomenon is also substantiated by the visible change of a darker and more black hair color at the root to a lighter and brownish color at the tip.

As mentioned earlier, streaming zeta potential for hair is much less explored and hence requires a detailed explanation. The zeta potential is an interface property that occurs when materials encounter liquids. The functional groups of the surface interact with the surrounding medium and a surface charge is created. The phenomenon can be better explained with the model of the electrochemical double layer (EDL) that consists of a stationary and a diffuse layer [26]. The stationary layer forms directly at the hair surface by the immobilized ions. The diffuse layer consists of ions in the solution that are less attracted to the surface and can move. The zeta potential (ζ) is defined as the sum of the original surface charge and the charge of the stationary layer.

The hair surface charge at the solid-liquid interface in an aqueous solution is generated by two main mechanisms: a) the acid-base reactions between the functional groups

and an aqueous solution and b) the adsorption of ions on the surface. There are different dissociable acidic groups such as carboxylic acid, sulfonic acid and hydroxyl groups on the hair surface which, in water, become negatively charged whereas basic groups such as primary, secondary, and tertiary amines are protonated and acquire a positive charge [27]. The resulting surface charge depends on the areal density of the surface groups and the pH value of the aqueous solution. The pH dependence of the zeta potential therefore provides information on the nature and strength of the functional groups present on hair.

The root part of the hair is, as observed from morphological characterization, covered by a hydrophobic lipid layer. Therefore, the functional groups on the surface are not exposed. That leads to a more hydrophobic surface. Here, the behavior of the streaming zeta potential is dominated by the second phenomenon, namely the absorption of hydroxide ions on the hydrophobic surface resulting in a negative zeta potential (**Fig. 8**). More towards the tip, the amount of lipid decreases, and surface functional groups encounter with the solution. One could now assume that due to the stronger negative charge, the zeta potential will become more negative. However, exactly the opposite phenomenon is observed, the zeta potential decreases in absolute amount. This is because of the negative charge of the groups; they repel each other, leading to the swelling of the scale layer and allowing more ionic solution to penetrate the hair. The change in protein conformation from rigid and regular α-helix and β-sheet to random coil facilitates the process. All these phenomena result in a shift of the shear plane that ultimately results in the change in the zeta potential curve. The IEP provides information about the composition of the functional groups that are present on the surface [28]. Completely hydrophobic surfaces have the IEP at a pH of 4. As the acidic functional groups on the hair surface get more and more exposed from root to tip, more acid is required to sufficiently protonate the functional groups of the hair surface to achieve a balance of positive and negative charges, i.e., the IEP.

TG analysis results (**Fig. 9**) fit perfectly with the results of the other analytical techniques used in this study. The different decomposition patterns indicate a difference in internal structure along the hair fibers [29, 30]. The most prominent change is observed for the peak responsible for keratin denaturation, which indicates that the weathering of hair influences the mass loss process. Hence the results are in agreement with the ATR-FTIR and

streaming zeta potential results, clearly depicting the hair keratin becoming more disorganized and permeable in nature during aging.

Conclusion.

This study deals with the detailed characterization of the aging of Indian hair. The chemically untreated hair helps to understand the effects of aging better. Morphological studies like LSM, SEM and AFM showed that the surface lipid concentration decreases, cuticular damage increases and hair becomes roughened as it grows and is exposed to weathering, all of which finally leads to the complete lifting of cuticles. We have carried out a detailed study to analyze the ATR-FTIR spectra better to understand the change on relative amounts of lipids and sulphur oxidation products but also to access the change in protein structure from regular structures at the root to an irregular one in the tip. The detailed streaming zeta potential studies help to complete the picture by showing the different water permeabilities of hair in root, length, and tip. Also, the different IEPs supports the idea of a different chemical nature of the hair parts that is further supported by the TG results. All these studies indicate a different spatial physical and chemical nature of the hair along the length. These results not only help to understand the Indian hair structure better but at the same time open up possibilities for further functionalization. Although this work is based on Indian hair, the analogy can still be applied for other hair types for future cosmetic applications for care, color and style.

Conflict of Interest Statement. NONE.

References.

1.   Robbins, C. R., **1988**, Chemical and Physical Behavior of Human Hair. Springer New York, NY.

2.   Popescu, C.; Hocker, H., Hair—the most sophisticated biological composite material. *Chem. Soc. Rev.* **2007,** *36*, 1282-1291.

3.   Keidel, I.; Neibecker, H.; Imdahl, I., The Importance of Hairstyle and Hair Care for Human Dignity. *SOFW J.* **2022,** *148*, 16-20.

4.   Langbein, L.; Yoshida, H.; Praetzel-Wunder, S.; Parry, D. A.; Schweizer, J., The Keratins of the Human Beard Hair Medulla: The Riddle in the Middle. *J. Invest. Dermatol.* **2010,** *130*, 55-73.

5.   Wei, G.; Bhushan, B.; Torgerson, P. M., Nanomechanical characterization of human hair using nanoindentation and SEM. *Ultramicroscopy* **2005,** *105*, 248-266.

6.   Hearle, J. W. S., A critical review of the structural mechanics of wool and hair fibres. *Int. J. Biol. Macromol.* **2000,** *27*, 123-138.

7.   Cruz, C. F.; Costa, C.; Gomes, A. C.; Matamá, T.; Cavaco-Paulo, A., Human Hair and the Impact of Cosmetic Procedures: A Review on Cleansing and Shape-Modulating Cosmetics. *Cosmetics* **2016,** *3*, 1-22.

8.   Fellows, A. P.; Casford, M. T. L.; Davies, P. B., Nanoscale Molecular Characterization of Hair Cuticle Cells Using Integrated Atomic Force Microscopy-Infrared Laser Spectroscopy. *Appl. Spectrosc.* **2020,** *74*, 1540-1550.

9.   Korte, M.; Akari, S.; Kühn, H.; Baghdadli, N.; Möhwald; Luengo, G.S., Distribution and Localization of Hydrophobic and Ionic Chemical Groups at the Surface of Bleached Human Hair Fibers. *Langmuir.* **2014,** *30*, 12124–12129.

10.   Franbourg, A.; Hallegot, P.; Baltenneck, F.; Toutain, C.; Leroy, F., Current research on ethnic hair. *J. Am. Acad. Dermatol.* **2003,** *48*, 1-5.

11.   Leerunyakul, K.; Suchonwanit, P., Asian Hair: A Review of Structures, Properties, and Distinctive Disorders. *Clin. Cosmet. Investig. Dermatol.* **2020,** *13*, 309-318.

12.   Trueb, R. M., From Hair in India to Hair India. *Int. J. Trichology.* **2017,** *9*, 1-6.

13.   Wolfram, L. J., Human hair: a unique physicochemical composite. *J. Am. Acad. Dermatol.* **2003,** *48*, 1-9.

14. Richena, M.; Rezende, C. A., Morphological degradation of human hair cuticle due to simulated sunlight irradiation and washing. *J. Photochem. Photobiol. B* **2016,** *161*, 430-440.

15. Fernandez, E.; Barba, C.; Alonso, C.; Marti, M.; Parra, J. L.; Coderch, L., Photodamage determination of human hair. *J. Photochem. Photobiol. B* **2012,** *106*, 101-106.

16. Wang, N.; Barfoot, R.; Butler, M.; Durkan, C., Effect of Surface Treatments on the Nanomechanical Properties of Human Hair. *ACS Biomater. Sci. Eng.* **2018,** *4*, 3063-3071.

17. Naudin, G.; Bastien, P.; Mezzache, S.; Trehu, E.; Bourokba, N.; Appenzeller, B. M. R.; Soeur, J.; Bornschlogl, T., Human pollution exposure correlates with accelerated ultrastructural degradation of hair fibers. *Proc. Natl. Acad. Sci. U.S.A.* **2019,** *116*, 18410-18415.

18. Stanic, V.; Maia, F. C. B.; Freitas, R. O.; Montoro, F. E.; Evans-Lutterodt, K., The chemical fingerprint of hair melanosomes by infrared nano-spectroscopy. *Nanoscale* **2018,** *10*, 14245-14253.

19. Zoccola, M.; Mossotti, R.; Innocenti, R.; I. Loria, D.; Rosso, S. and Zanetti, R., Near Infrared Spectroscopy as a Tool for the Determination of Eumelanin in Human Hair. *Pigment Cell Res.* **2004,** *17*, 379–385.

20. Takahashi, T.; Mamada, A.; Breakspear, S.; Itou, T.; Tanji, N., Age-dependent changes in damage processes of hair cuticle. *J. Cosmet. Dermatol.* **2015**, *14*, 2-8.

21. Coderch, L.; Oliver, M. A.; Martínez, V.; Manich, L.; M. Martí, R., *Skin Res Technol.* **2017**, *23*, 479–485.

22. Okamoto, M.; Ishikawa, K.; Tanjia N.; Aoyagib, S., Investigation of the damage on the outermost hair surface using ToF-SIMS and XPS. *Surf. Interface Anal.* **2012**, *44*, 736–739.

23. Tokunaga, S.; Tanamachi, H.; Ishikawa; K., Degradation of Hair Surface: Importance of 18-MEA and Epicuticle. *Cosmetics* **2019**, *6*, 31.

24. Luengo, G. S.; Greaves, A. J., **2021**, Surface Science and Adhesion in Cosmetics. Scrivener Publishing LLC, Beverly, United States.

25. Ito, S.; Wakamatsu, K.; Sarna, T., Photodegradation of Eumelanin and Pheomelanin and Its Pathophysiological Implications. *Photochemistry and Photobiology* **2018**, *94*, 409–420.

26. Lyklema, J., Surface Conduction. *J. Condens. Matter Phys.* **2001,** *13,* 5027.

27. Luxbacher, T., **2020**, Handbook of Natural Fibres (Second Edition), Elsevier Ltd., Amsterdam, Netherlands.

28. Parriera, H. C., On the Isoelectric Point of Human Hair. *J. Colloid Interface Sci.* **1980**, *75*, 212-217.

29. Monteiro, V. F.; Maciel, A. P.; Longo, E., Thermal Analysis of Caucasian Human Hair. *J. Therm. Anal. Calorim.* **2005**, *79*, 289–293.

30. Mohan, N. H.; Ammayappan, L.; Sarma, D. K.; Debnath, S.; Tamuli, M. K., Characterization of Thermal Properties of Pig Hair Fiber. *J. Nat. Fibers* **2017**, 14, 459-465